

## The Science Case for PILOT II: the Distant Universe

*J.S. Lawrence<sup>A,J</sup>, M.C.B. Ashley<sup>A</sup>, A. Bunker<sup>B</sup>, R. Bouwens<sup>C</sup>, D. Burgarella<sup>D</sup>, M.G. Burton<sup>A</sup>, N. Gehrels<sup>E</sup>, K. Glazebrook<sup>F</sup>, K. Pimbblet<sup>G</sup>, R. Quimby<sup>H</sup>, W. Saunders<sup>B</sup>, J.W.V. Storey<sup>A</sup>, J.C. Wheeler<sup>I</sup>*

<sup>A</sup> School of Physics, University of New South Wales, NSW 2052, Australia

<sup>B</sup> Anglo-Australian Observatory, NSW 1710, Australia

<sup>C</sup> Department of Astronomy and Astrophysics, University of California Santa Cruz, Santa Cruz, CA 95064, USA

<sup>D</sup> Observatoire Astronomique de Marseille Provence, Université d'Aix-Marseille, Marseille 13388, France

<sup>E</sup> NASA/Goddard Space Flight Center, Greenbelt, MD 20771, USA

<sup>F</sup> Centre for Astrophysics and Supercomputing, Swinburne University of Technology, Hawthorn, VIC 3122, Australia

<sup>G</sup> Department of Physics, University of Queensland, Brisbane, QLD 4072, Australia

<sup>H</sup> Astronomy Department, California Institute of Technology, Pasadena, CA 91125, USA

<sup>I</sup> Department of Astronomy, University of Texas, Austin, TX 78712, USA

<sup>J</sup> JSL now at Department of Physics and Electronic Engineering, Macquarie University, NSW 2109, Australia; and Anglo-Australian Observatory, NSW 1710, Australia; Email: jsl@physics.mq.edu.au

**Abstract:** PILOT (the Pathfinder for an International Large Optical Telescope) is a proposed 2.5 m optical/infrared telescope to be located at Dome C on the Antarctic plateau. The atmospheric conditions at Dome C deliver a high sensitivity, high photometric precision, wide-field, high spatial resolution, and high-cadence imaging capability to the PILOT telescope. These capabilities enable a unique scientific potential for PILOT, which is addressed in this series of papers. The current paper presents a series of projects dealing with the distant (redshift  $> 1$ ) Universe, that have been identified as key science drivers for the PILOT facility. The potential for PILOT to detect the first populations of stars to form in the early Universe, via infrared projects searching for pair-instability supernovae and gamma-ray burst afterglows, is investigated. Two projects are proposed to examine the assembly and evolution of structure in the Universe: an infrared survey searching for the first evolved galaxies at high redshift, and an optical survey aimed at characterising moderate-redshift galaxy clusters. Finally, a large-area weak-lensing survey and a program to obtain supernovae infrared light-curves are proposed to examine the nature and evolution of dark energy and dark matter.

**Keywords:** telescopes — early universe — galaxies: high-redshift — cosmology: observations — large-scale structure of universe — supernovae: general — galaxies: clusters: general

## 1 Introduction

PILOT (Pathfinder for an International Large Optical Telescope) is proposed as a high spatial resolution wide-field telescope with an optical design and an instrument suite that are matched to the Dome C atmospheric conditions. These conditions have been shown to offer high infrared sensitivity, due to the low atmospheric thermal emission and low water-vapour column-density (Lawrence 2004; Walden et al. 2005; Tomasi et al. 2006); high spatial resolution and high photometric precision, due to the unique atmospheric turbulence structure above the site (Lawrence et al. 2004; Agabi et al. 2006; Kenyon et al. 2006; Trinquet et al. 2008); and a high cadence, due to the high latitude of the site and the high percentage of cloud-free condi-

tions (Kenyon & Storey 2006; Mosser & Aristidi 2007).

The scientific justification for the PILOT telescope has evolved from earlier work (Burton et al. 1994, 2001, 2005) in parallel with the telescope and instrument suite design (Saunders et al. 2008a,b). The PILOT science case is presented here in a series of three papers. Paper I (Lawrence et al. 2009a) gives a summary of the science case, and an overview of the project (including the telescope design, expected performance, and observing strategies). The current paper (Paper II) presents a series of science projects for the PILOT facility that are aimed at observing and understanding the distant Universe (i.e., beyond a redshift of  $z \approx 1$ ). Paper III (Lawrence et al. 2009b) discusses PILOT science projects dealing with the nearby Universe (i.e., the Solar System, the Milky Way, and nearby galax-

ies).

The baseline optical design for PILOT, described in Saunders et al. (2008a), comprises a 2.5 m Ritchey-Chretien telescope with an f/10 overall focal ratio. The telescope is housed in a temperature- and humidity-controlled dome that is mounted on top of a  $\sim 30$  m high tower in order to elevate the main mirror above the majority of the intense ground-layer turbulence. A fast tip-tilt secondary mirror is used for guiding and to remove residual boundary-layer turbulence and tower wind-shake. As detailed in Paper I (see also Saunders et al. 2008b) the baseline instrument suite for PILOT includes the PILOT VISible Camera (PVISC), a wide-field ( $40' \times 40'$ ) optical imaging camera with a spatial resolution of  $\sim 0.3''$  over the wavelength range  $0.4\text{--}1\ \mu\text{m}$ ; the PILOT Near-InfraRed Camera (PNIRC), a wide-field ( $10' \times 10'$ ) near-infrared camera achieving a similar spatial resolution over the wavelength range  $1\text{--}5\ \mu\text{m}$ ; the PILOT Mid-InfraRed Imaging Spectrometer (PMIRIS), a wide-field ( $40' \times 40'$ ) mid-infrared instrument operating from  $7\text{--}40\ \mu\text{m}$ , with several spectral-resolution modes; and the PILOT Lucky Imaging Camera (PLIC), a fast optical camera for diffraction-limited imaging over relatively small-fields ( $0.5' \times 0.5'$ ) in the visible.

The “distant Universe” science cases described in this paper are divided into three key themes: *first light in the Universe*, *the assembly of structure*, and *dark matter and dark energy*. The projects proposed under these themes have been identified to take advantage of the unique discovery space of the PILOT telescope, enabled by the Dome C site conditions and the telescope design. For each project, the context and impact is discussed, along with the capabilities of competing (and synergistic) facilities. Additionally, the observational requirements are identified. It is shown that the observational requirements for these projects can either only be achieved with PILOT or can be achieved with other facilities but with much lower efficiency. While many of the science projects described here (and in Paper III) require large amounts of observing time (several seasons in some cases), the observing strategies proposed in Paper I should allow the majority of these science projects to be completed within the proposed ten-year lifetime of the PILOT facility.

*First light in the Universe* (Section 2) projects are linked by the desire to detect and characterise the earliest stellar populations to form. Here, we investigate the potential for PILOT to observe the signatures of the final evolutionary stages of very high-redshift (i.e.,  $z > 10$ ) Population III super-massive stars. A deep wide-area infrared survey should allow the detection of pair-instability supernovae. A target-of-opportunity program of near- to mid-infrared satellite-alert follow-up should allow the detection of gamma-ray burst afterglows.

*The assembly of structure* theme (Section 3) links studies of distant galaxies and galaxy clusters. We investigate the potential for PILOT to detect distant galaxies via deep, wide-field, infrared surveys at  $K_d$ -band. In particular, the first populations of evolved galaxies to form, in the redshift range  $z = 5\text{--}7$ , should be identifiable with PILOT, when combined with other

telescope survey data, via photometric observations around the redshifted Balmer break wavelength. We also propose an optical investigation of a significant number of X-ray selected galaxy clusters in the redshift range  $z = 0.6\text{--}1.5$ . This study will further our understanding of cluster growth, structure, and evolution.

The *dark matter and dark energy* theme (Section 4) involves two projects that aim to investigate the evolution of cosmological parameters. Firstly, a very wide-area optical sky survey is proposed to measure large-scale structure via the weak-lensing signature of distant galaxies. From this structure, constraints on the nature and evolution of dark matter and dark energy can be derived. Secondly, a PILOT survey aimed at obtaining large numbers of supernovae Ia light-curves at near-infrared wavelengths, where they are largely unaffected by dust extinction and reddening, will play an important role in removing (or confirming) concerns that dust may affect current constraints placed on cosmological parameters from optical data.

## 2 First Light in the Universe

### 2.1 Pair-Instability Supernovae at High Redshift

#### 2.1.1 Impact

Pair-instability Supernovae (PISNe) are predicted to be extremely powerful thermonuclear explosions that result from the softening of the equation of state by electron/positron pair formation and the subsequent contraction, heating, ignition, and total disruption of the oxygen cores of especially massive stars. Current theoretical estimates of the progenitor mass range and resulting explosion energy are  $140$  to  $250\ M_{\odot}$  and  $2 \times 10^{51}$  to  $100 \times 10^{51}$  ergs, respectively (Heger & Woosley 2002). Conditions in the early Universe at high redshift are predicted to be especially conducive to the formation of such massive stars (Bromm & Larson 2004). The existence and distribution with redshift of PISNe may thus provide a powerful way of probing the history of chemical enrichment and reionisation and of the physical conditions in the environments around the first structures to form in the Universe.

The pair-instability process is predicted to occur for massive stars in very low metallicity environments. The metal-free environment lowers the fragmentation of collapsing clouds, therefore resulting in larger protostellar cores (e.g., Abel et al. 2002). It also increases the accretion rates that are not arrested by the processes of radiation pressure, bipolar outflows, and rotation. Finally, it suppresses the efficiency of line-driven wind mass loss so that massive stars do not shed their hydrogen envelopes before core He burning is ended (Kudritzki 2002). These factors lead to the large stellar masses essential for the pair-instability process. The low metallicities required suggest that PISNe should be numerous amongst the first (Population III) stars.

For stars in the appropriate mass range, the pair-instability process involves the complete disruption of

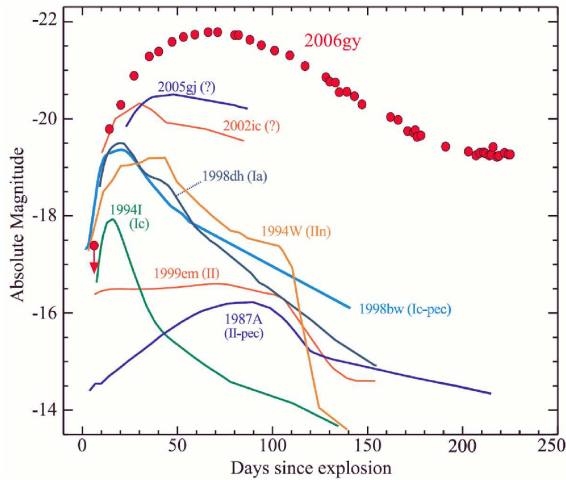


Figure 1: Absolute  $R$ -band light-curve for SN2006gy compared with those of other SNe (types indicated in figure). From Smith et al. (2007).

the progenitor. In this case the whole core of the star (20–60  $M_{\odot}$ ) is converted to radioactive  $^{56}\text{Ni}$ , creating an object that is intensely bright, typically  $-22$  absolute mag, and lasting for typically 50–150 days. For stars of mass lower than  $\sim 140 M_{\odot}$  the nuclear burning initiated by the pair instability is not sufficient to halt the collapse; such objects thus leave behind a black hole remnant (Heger & Woosley 2002). Stars of initial mass greater than  $\sim 250 M_{\odot}$  are thought to collapse via photo-disintegration, also leaving a blackhole remnant (Heger & Woosley 2002).

As the PISN process involves the complete disruption of the progenitor star, and since they should be numerous amongst Population III stars formed in the range  $z \approx 10$ –20, this process is thought to be primarily responsible for enriching the IGM metallicity above the critical level sufficient to halt very massive star formation and allow Population II stars to form (e.g., Scannapieco et al. 2003). However, metal enrichment is a local process that is not expected to raise metallicity in a completely homogeneous way. For this reason, it is expected that PISN should occur at much lower redshifts (to a least  $z = 6$ ) in isolated regions of gas where metals have not yet propagated (Mackey et al. 2003). There is, as yet, no sign of the specific chemical signature of PISNe in abundance studies of low metallicity stars, but this may be due to selection effects (Karlsson et al. 2008).

Models predict that PISNe will be observationally distinct from other SNe since they are much more luminous, exhibit a much slower rise time to peak luminosity, and stay brighter for a longer time. SN 2006gy, the light curve of which is shown in Figure 1, is a recently discovered local (within  $\sim 100$  Mpc) SN which meets these characteristics (Smith et al. 2007). This SN took  $\sim 70$  days to reach peak luminosity, compared with  $\sim 20$  days typical for other SN types, and reached

a peak absolute brightness of  $-22$  magnitudes, a factor 2–6 times brighter than other SN types. Woosley et al. (2007) suggested that this object could be a pulsational type of PISN. More recent work, however, suggests alternative explanations (Smith & McCray 2007; Smith et al. 2008).

## 2.1.2 Observing Strategies and Detection Rates

No confirmed detection of a PISN has yet occurred. As these objects are theoretical predications based on extrapolations from existing data and models, there is a large uncertainty as to their expected characteristics. A wide range of expected number densities of PISNe have been reported. Values range from 1 to 36 objects per  $\text{deg}^2$  per year per unit redshift at  $z = 6$ , and from 0.3 to 6 objects per  $\text{deg}^2$  per year per unit redshift at  $z = 15$  (Scannapieco et al. 2005; Weinmann & Lilly 2005; Wise & Abel 2005). This large range arises from uncertainties in several of the model input parameters, primarily the fraction of gas per primordial object converted into stars (i.e., the star formation rate, SFR), the number of PISNe per unit mass of stars formed, and the mass distribution for Population III stars (i.e., the initial mass function, IMF). There is also a large range of predicted values for the PISN rest-frame ultraviolet time interval, specified as the time the event is one magnitude brighter than the peak brightness, from a few days (Heger et al. 2002; Weinmann & Lilly 2005) to  $\sim 30$  days (Scannapieco et al. 2005) to  $\sim 100$  days (Wise & Abel 2005). This corresponds to an observed-frame time interval ranging from a few tens of days at low redshift to more than a year for very high-redshift objects. Finally, there is a range of expected absolute peak brightness for these objects, ranging from  $-20$  to  $-24$  for progenitor masses of  $250 M_{\odot}$  (Scannapieco et al. 2005; Weinmann & Lilly 2005; Wise & Abel 2005) arising because of the range of simplifying assumptions used in the models. These uncertainties will have significant implications for the observing strategy and required cadence for any PISN search. If the values for the time interval are at the upper end of the expected range, then multi-year programs will be essential. If the values for the peak brightness are at the lower end of the expected range, then very long integrations will be required per field.

For relatively low-redshift PISNe, a search in  $i$ -band, above the limit for Lyman  $\alpha$  absorption at  $z \approx 5$ , is appropriate. The required sensitivity for detection is  $m_{AB} \approx 27$  (Scannapieco et al. 2005). Such a search would require an integration time per field of  $\sim 1.8$  hours for PILOT’s PVISC instrument. For a dedicated survey (i.e., 100% of telescope time spent on this project), a 3000 hour search (i.e., one winter season) would allow over  $800 \text{ deg}^2$  to be covered. This would be expected to find thousands of PISN in the range  $z = 2$ –3 and a few tens of PISN out to  $z = 4$  (Scannapieco et al. 2005), assuming that these objects exist at such low redshifts. Other ground-based wide-area optical survey facilities such as LSST and Pan-STARRS-4 should be capable of similar detection rates at this wavelength, but only if they spend much longer, and go much deeper, than

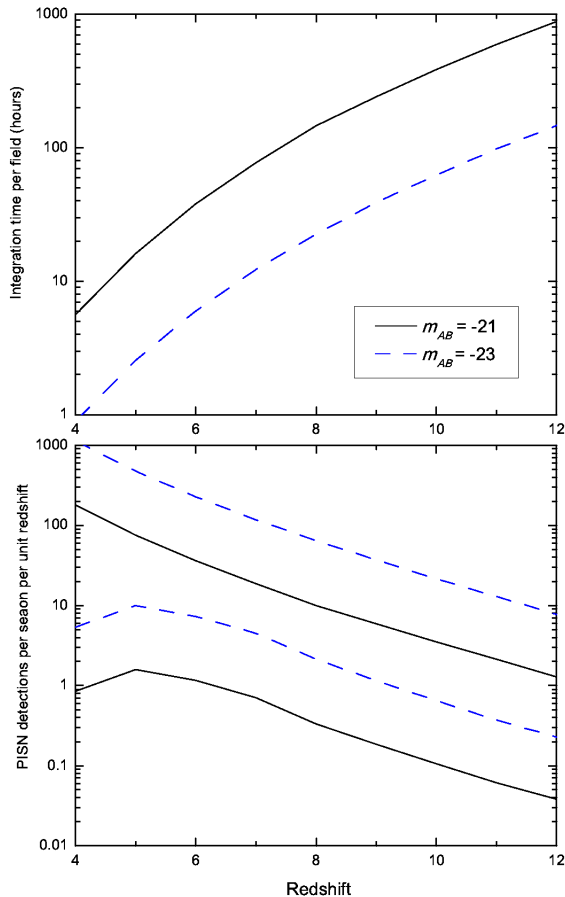


Figure 2: Top: integration time required per field for PISN detection 0.5 magnitudes below peak brightness at  $K_d$ -band with PNIRC for PISN absolute brightness of  $m_{AB} = -21$  and  $-23$ . Bottom: expected number of PISNe detected by PILOT per winter season (3000 hours) as a function of redshift for a dedicated  $K_d$ -band survey, for PISN absolute brightness of  $m_{AB} = -21$  and  $-23$ . In each case, the upper and lower detection limits are based on PISN number density estimates from Scannapieco et al. (2005) and Weinmann & Lilly (2005). A rest-frame ultraviolet time interval of 20 days, and a search pattern that repeats at the corresponding observed-frame time interval, is assumed. Multi-year searches will thus be required to find very high-redshift objects.

their currently planned survey strategies.

A more promising opportunity for PILOT is to search for higher-redshift PISNe in the near-infrared  $K_d$ -band with PNIRC. Figure 2 shows the required integration time for PISNe with an absolute brightness ranging from  $m_{AB} = -21$  to  $-23$ , and the expected detection rate per season as a function of redshift. For PISNe at the upper end of the expected range of brightness, integration times per field range

from 1 hour at  $z = 4$ , to 50 hours at  $z = 10$ , corresponding to total search areas of  $3\text{--}90 \text{ deg}^2$  (i.e., before repeat visits are required). Using pessimistic surface density predictions, PILOT should detect at least one PISN at  $z \approx 10$  per season. Optimistic models allow the detection, per season, of several hundred PISN in the range  $z = 6\text{--}10$ , and at least one beyond  $z = 12$  (for very long integrations). For PISN at the lower end of the expected range of brightness, much longer integration times are required, resulting in very small search areas and a low probability of detecting any PISN at redshifts greater than about  $z = 8$ . SN2006gy type objects (with peak brightness of  $m_{AB} \approx -22$ ) should be discovered at least out to  $z = 6$ , and possibly hundreds could be discovered per season. While there are large uncertainties associated with these predictions, they illustrate the potential for PILOT in this area.

Other transient phenomena will also be detected by the PISN survey, and while these may comprise an interesting sample in their own right, they represent contaminants to the PISN sample that must be identified and excluded. This can effectively be done by breaking up the long integrations into multiple epochs and with supporting multi-band observations of the host galaxies. It is difficult or impossible to differentiate between a high-redshift PISN and a low-redshift transient, such as a Type Ia SN, given only a single detection from a very long  $K_d$  exposure; however, if the integration were broken up over several weeks, then each epoch would sample a photometrically distinct portion of the Type Ia supernova’s light curve, but the slowly evolving PISN would remain essentially constant. Similarly, AGN exhibit a red-noise power spectral distribution and may be seen to vary across the multiple epochs. However, some Type II SNe can show nearly constant photometric plateaus, and  $z = 1.5$  Type II-P supernova could have the same peak apparent brightness as a  $z = 10$  PISN. Such contaminants may be further weeded out by comparison with deep template images. An  $R$ -band detection of the host, for example, would place the transient at  $z < 5$ . If the template images extended into multiple bands, a photometric redshift could further refine the distance. Finally, multi-epoch high-resolution spectroscopic follow-up of any PILOT PISN detection using 8-m class mid-latitude telescopes (and/or JWST) will help refine redshift estimates for these objects.

### 2.1.3 Other Facilities

The faintness of PISNe in the infrared and their inherent rarity calls for a very specialised facility to detect them. As indicated here, it requires a telescope with a wide field-of-view and a high infrared sensitivity. This is a good match to the capabilities of PILOT. The expected rarity of these events demonstrates the importance of field-of-view. This science case would be significantly strengthened, for example, by increasing the field-of-view of PNIRC by a factor of 4 (i.e., using a larger mosaic of detectors).

The  $K_d$ -band is chosen here to illustrate the potential for PILOT to detect high-redshift PISNe as this is the most efficient wavelength to search in the

near-infrared (PILOT should observe to a depth of 0.3 and 0.7 AB magnitudes fainter at  $K_d$ -band than at  $J$ -band and  $H$ -band respectively). The  $K_d$ -band is also where PILOT has the largest advantage compared to mid-latitude telescopes; PILOT is a factor of eight times faster to reach a given depth over a given area at this wavelength than VISTA, for example. For a mid-latitude telescope, however, it is more efficient to observe at  $J$ -band or  $H$ -band than at  $K$ -band and PILOT is only marginally more sensitive at these lower wavelengths. The real benefit to a PISN search at  $K_d$ -band is thus the possibility to detect higher redshift objects that cannot be observed at lower wavelengths.  $J$ -band and  $H$ -band correspond to Lyman  $\alpha$  redshifted to  $z = 10$  and  $z = 13$  respectively. Peak spectral emission for PISN is expected to occur at wavelengths longer than Lyman  $\alpha$  (Scannapieco et al. 2005). Mid-latitude ground-based telescopes are thus precluded from detecting significant numbers of these objects at redshifts beyond about  $z = 6 - 8$ .

While JWST is much more sensitive in the thermal infrared than PILOT (it should reach  $m_{AB} = 28$  at  $2.5 \mu\text{m}$  for  $R = 10$  in  $\sim 13$  minutes<sup>1</sup>), the infrared camera NIRCcam has a smaller field-of-view than PNIRC. Additionally, the time associated with slewing and settling precludes JWST from conducting surveys over large (degree scale) regions of sky. PILOT will thus probe a different region of the possible PISN parameter space. If PISNe occur at the faint end of the expected brightness range and are common, then only JWST will find them at high redshift (Gardner et al. 2006). If PISNe occur at the bright end of the expected brightness range with low surface density, then JWST will not be able to cover a sufficient area of sky and PILOT will be the only facility capable of detecting them (JWST will then be a useful facility for following up any such PILOT detections). If these objects, however, are both very faint and very rare, then detection of high-redshift PISNe will not be possible with any currently envisaged telescope.

## 2.2 High-Redshift Gamma-Ray Bursts

### 2.2.1 Impact

Gamma-ray bursts (GRBs) are extremely powerful explosions, with total energies ranging from  $3 \times 10^{51}$  to  $2 \times 10^{54}$  ergs. They are rare astrophysical events believed to be produced by internal shocks taking place in a collimated jet of relativistic particles that is emitted by a central engine. Satellite observations have demonstrated a bimodal temporal distribution to this high-energy emission (Kouveliotou et al. 1993). Short “hard” bursts (lasting less than  $\sim 2$  seconds) have been attributed to the coalescence of binary compact objects in nearby galaxies (Fox et al. 2005; Gehrels et al. 2005). Long-duration bursts (lasting less than a few minutes) have been associated with the gravitational core-collapse of massive stars in distant galaxies (MacFadyen & Woosley 1999). In both cases the interaction of the jet with the surrounding medium produces an afterglow of much

longer duration, typically lasting hours to days (Akelof et al. 1999; Nousek et al. 2006; Zhang et al. 2006). This afterglow, observed at optical, X-ray, and radio wavelengths, is thought to be less directional than the high-energy (gamma-ray) emission. It is thus expected that geometries will exist that result in the detection of an “orphan” afterglow (i.e., unaccompanied by gamma-ray emission). Approximately 40% of GRBs are known to be “dark bursts”, i.e., they have no optical counterpart to faint limits. This is believed to occur for cases of high obscuration, where the optical emission is attenuated, and high redshift, where the optical emission falls at a shorter wavelength than the Lyman  $\alpha$  cut-off in the source frame.

Due to their high intrinsic luminosity, gamma-ray bursts offer a powerful probe of the Universe at a range of cosmological distances. Both the host-galaxy interstellar medium and the intergalactic medium are imprinted on the spectrophotometric signature of the gamma-ray burst optical/infrared afterglow (Prochaska et al. 2007). Their association with the final stages of the evolution of massive stars provides information on the star formation history of the Universe at different cosmological eras (Jakobsson et al. 2005). The highest redshift GRB so far detected is at  $z = 6.3$  (Kawai et al. 2006). Theories suggest that long duration GRBs should be numerous at higher-redshifts in the range  $z = 10-20$  (Lamb & Reichart 2000), and should thus have Population III progenitors. These afterglows will be both highly time-dilated and severely reddened. They provide an important tool to probe the evolution of the ionisation state and metallicity of the Universe, and the physical properties of the first stars to form. Additionally, evidence suggests that some long duration GRBs are associated with Type Ib/Ic supernovae (e.g., Woosley & Bloom 2006).

Even in the current Swift era, there is a paucity of uniform optical afterglow observations of GRBs. Many of the interesting gamma-ray triggers from Swift and other satellites, including high-redshift candidates, are not adequately observed. Also, there is great interest in detecting orphan afterglows that are expected to occur at higher rates than normal afterglows (Totani & Panaitescu 2002; Zou et al. 2007) and provide valuable information on beaming.

### 2.2.2 Other Facilities

The Swift gamma-ray satellite, which currently finds  $\sim 100$  GRBs per year and provides a location accuracy of  $\sim 3''$  within a few minutes for a large fraction of these (Gehrels et al. 2004), has an orbital lifetime to  $\sim 2020$  and is funded through 2012 with extensions possible after that. The Gamma-ray Large Area Space Telescope (GLAST) was launched in January 2008 with a lifetime of 5–10 years and is expected to find  $\sim 50$  GRBs per year with a location accuracy of  $\sim 10'$  with the LAT instrument, and a further  $\sim 150$  GRBs per year with an accuracy of  $\sim 10^\circ$  with the GBM instrument (von Kienlin et al. 2004). Future GRB space missions, such as the Space multi-band Variable Object Monitor (SVOM), the Explorer of Diffuse Emission and Gamma-ray burst Explosions (EDGE), and the En-

<sup>1</sup>Based on scaling the quoted JWST sensitivity limits at <http://www.stsci.edu/jwst/science/sensitivity/>

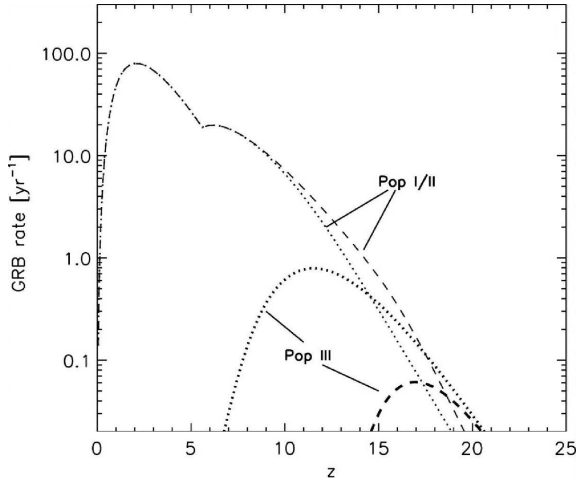


Figure 3: Predicted GRB rates observed by Swift as a function of redshift for Population I, II, and III progenitors. The Population III rate includes strong and weak feedback models, dashed and dotted lines respectively. From Bromm & Loeb (2006).

energetic X-ray Imaging Survey Telescope (EXIST) are each expected to find several hundred GRBs per year with location accuracies ranging from 1–10' (den Herder et al. 2007; Band et al. 2008).

Salvaterra et al. (2008) have recently estimated the expected number of high-redshift satellite GRB detections based on models of the luminosity function and formation rate for long duration GRBs. These models predict that Swift should find 3–16 GRBs per year at  $z \geq 6$ , and 0.3–0.9 GRBs per year at  $z \geq 10$ . Models from Bromm & Loeb (2006), shown in Figure 3, are more optimistic, and also predict that the number of high-redshift GRBs arising from Population III progenitors could be significant. The analysis of Salvaterra et al. (2008) showed that GLAST is only expected to find a few GRB per year at  $z \geq 6$ , and has a low probability of finding any GRBs at  $z \geq 10$ . SVOM, EDGE, and EXIST are more appropriate to high-redshift detections, however, and should find 2–50 per year at  $z \geq 6$ , and 0.1–3 per year at  $z \geq 10$ .

There are a number of ground-based facilities that are capable of responding to such GRB satellite alerts and performing optical/near-infrared follow-up. These include dedicated telescope networks, such as ROTSE, dedicated survey telescopes, such as VISTA, and general purpose 8–10 m class telescopes (Keck, Gemini, VLT, etc). The applicability of such facilities to high-redshift GRB afterglow detection is limited, however, thermal infrared sensitivities (due to atmospheric thermal emission), and the availability and wavelength coverage of near- and mid-infrared instruments on 8 m class telescopes. This is evidenced by that fact that although Swift has probably detected many high-redshift GRBs according to the predictions of Salvaterra et al. (2008), only  $\sim 30\%$  of Swift bursts have redshift deter-

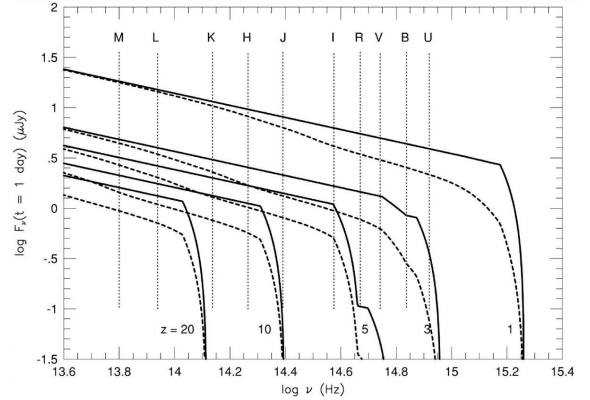


Figure 4: Spectral flux distribution of GRB970228, as observed one day after the burst, after transforming it to various redshifts and extinguishing with a model of the Ly- $\alpha$  forest. From Lamb & Reichart (2000).

minations. Many bursts with stretched out gamma-ray light curves that appear to be at high redshift have either not been optically followed-up or have been followed up only at visible wavelengths with no detection. There is thus a great potential here that needs rapid infrared follow-up to realize.

There are also a number of ground-based projects with aims to independently search for GRB orphan afterglows, such as LSST and VISTA. With very large fields-of-view, these facilities are well suited to searching for such objects. Again, however, long wavelength cut-offs and thermal infrared sensitivities will preclude these facilities from finding orphan afterglows originating from very high-redshift sources.

PILOT will not be competitive with LSST for finding low-redshift orphan-afterglows in the visible, as spatial resolution is not critical and LSST is  $\sim 25$  times faster to a given depth. PILOT may, however, be uniquely suited for orphan afterglow searches in the near-infrared: it should be  $\sim 8$  times faster than VISTA at  $K$ -band and has a wider wavelength range. These objects are expected to be very rare, however. More experimental data are needed to constrain the expected rates for orphan afterglows; none have so far been detected, and there are large uncertainties (3–4 orders of magnitude) in the predictions on the expected number density (e.g., Totani & Panaitescu 2002; Zou et al. 2007).

### 2.2.3 Observing Strategies

The key role for PILOT will be to respond quickly to either satellite or ground-based GRB detections, and follow up rapidly in the near- to mid-infrared (from 1–5  $\mu\text{m}$ ). The high sensitivity in the thermal infrared, the wide infrared wavelength range, and the potential to respond quickly and observe for long periods, means that PILOT is well suited to finding high-redshift GRBs. Space-based infrared telescopes, such as JWST, have

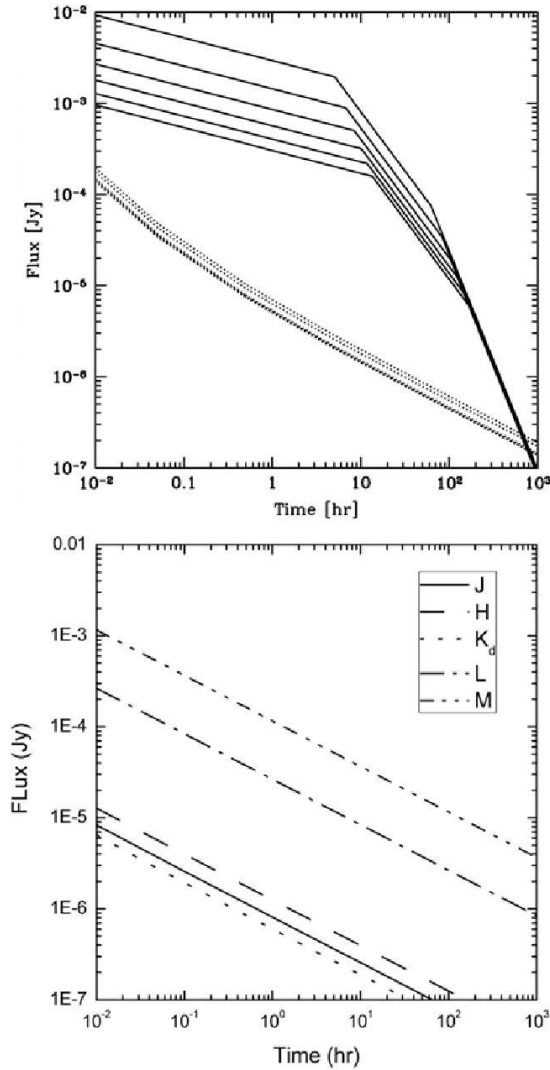


Figure 5: Top: high-redshift GRB afterglow flux (solid curves) as a function of time since the GRB explosion. Dotted curves show the  $R = 5000$  spectral detection threshold for the near-infrared spectrometer on JWST. Both sets of curves show redshift  $z = 5, 7, 9, 11, 13, 15$  (top to bottom respectively). From Barkana & Loeb (2004). Bottom: PILOT PNIRC detection threshold in  $J, H, K_d, L, M$  bands. For both plots, the integration time is 20% of the time since the burst.

an enormous advantage in terms of infrared sensitivity, but have a slow response time, and their smaller field-of-view can make burst location problematic.

While the effects of distance and redshift act to reduce the flux of a GRB at a fixed wavelength, time dilation acts to increase it at a fixed time of observation from onsets. Thus, in a given spectral band, there is little decrease in the intensity with redshift at a fixed time after the explosion. Based on fitting the spec-

tral energy distribution to one GRB, Lamb & Reichart (2000) estimate that the flux, one day after burst, will range from 10–20  $\mu\text{Jy}$  in  $K, L,$  and  $M$  bands for redshifts from  $z = 3$ –20 (except for  $K$ -band at  $z = 20$ , when the flux is shifted out of the band), as shown in Figure 4. In 5 minutes of observation, PILOT should be able to detect these objects with a  $SNR > 10$  at  $K_d$  and a  $SNR \approx 1$  at  $L$  and  $M$ . At earlier times, with the flux estimated to vary as  $t^{-4/3}$ , higher  $SNRs$  would be anticipated. Within the first hour of the burst they should readily be detectable. This suggests a filter sequence for a search for GRBs, from  $J$ , through  $H, K_d, L,$  to  $M$ , starting with 1–2 minutes at  $J$  and  $H$ . If no object is detected, then 5–10 minutes would be spent at  $K_d$ , rising to an hour at  $M$ . A GRB found only in  $M$ -band would have  $z > 30$ . Later models from Barkana & Loeb (2004) shown in Figure 5, and also Gou et al. (2004) and Inoue et al. (2007), give a significantly higher expected flux for high-redshift GRBs; events at this level could thus be followed for several days.

As shown here, PILOT should be capable of detecting very high-redshift GRB afterglows. The likelihood of such detections will ultimately be determined by the number of high-energy satellite alerts. A few hundred satellite detections per year are expected over the whole sky. If PILOT could follow-up in the near-infrared every GRB alert in the observable sky at Dome C during winter (i.e., about one a week) within  $\sim 10$  minutes, it should find several  $z > 6$  GRBs per season and at least one  $z > 10$  GRB in a few years. The distance to these objects can be determined via the Lyman  $\alpha$  drop-out wavelength. This will provide a tight constraint on the occurrence of GRBs in the early Universe. Additionally, as a by-product of other PILOT wide-field  $K_d$  survey projects, the rate of occurrence of high-redshift GRB orphan-afterglows will be probed to lower number densities than possible with any other facility.

## 3 Assembly of Structure

### 3.1 High-Redshift $K_d$ Galaxy Surveys

#### 3.1.1 Impact

The study of galaxy formation and evolution through cosmological history was revolutionised in 1995 with the observation of the first of the Hubble Deep Fields (HDF; Williams et al. 1996). Staring at a field in Ursa Major about  $2'$  across, over a period of ten days and through four broadband filters ranging from the near-ultraviolet to the near-infrared, over 3000 galaxies were identified. While many were clearly recognisable as spirals, there were also a larger proportion of disturbed and irregular galaxies than seen in the local Universe. The HDF also showed that the star formation rate was clearly higher in the past, and that galaxy collisions and mergers were more common than today. Subsequent studies have now made it clear that galaxies cover the sky with number densities of up to one per square arc-second, star formation rates peaked around

$z = 1-4$ , and our view of the Universe at this epoch is one of great disturbance.

Such deep fields are, however, inherently biased. In the optical they sample the rest-frame ultraviolet-light for galaxies that have  $z > 1$ . This makes them sensitive to where the most active star formation is taking place at these epochs; i.e., the ultraviolet radiation produced by young, luminous OB stars spread about their host galaxies (with an unknown distribution) dominates the view we see. The HDF at high redshift is thus dominated by Lyman-break galaxies (LBG). The light from the bulk of the stellar population—older, redder stars—is not seen, for this is redshifted out of the optical bands. It is necessary to look into the infrared to see this light.

The longest waveband where deep observations can be made from ground-based observatories is  $K$ -band (i.e., from 2.0–2.4  $\mu\text{m}$ ); at longer wavelengths the thermal emission from both the atmosphere and the telescope rises rapidly. In order to see the bulk of the light from evolved stars, it is necessary to observe at wavelengths beyond the rest-frame for the 4000 Å and Balmer breaks. For  $z > 3$ , this means  $K$ -band is essential.

The HST-NICMOS observations of the Hubble Deep Field South (HDF-S) identified 6% of the galaxies as having a photometric redshift  $z > 5$ , with another 3% as being evolved E/SO galaxies. Most of these galaxies could have been identified from purely optical deep fields. The deepest  $K$ -band image to date was taken in the HDF-S field, as part of the VLT-FIRES survey (Labbe et al. 2003). As the authors comment, there is a striking variety in optical-to-infrared colours across the field, especially for the fainter (more distant) objects. Many of the sources with red colours have photometric redshifts  $z > 2$  and are candidates for being massive, evolved galaxies. They would not have been identified by the traditional  $U$ -band dropout technique applied to the optical HDFs, for they are too faint in these bands.

While it appears that around two-thirds of the star formation in the Universe has occurred since  $z < 2$ , the remaining third has occurred at earlier epochs (e.g., Glazebrook et al. 2004). Much research in this field is directed to understanding when and how these stars formed, and what this implies for hierarchical models of galaxy formation. It is important to ascertain which population of galaxies hosts the star formation as a function of cosmic epoch. PILOT can address this directly by measuring stellar masses at high redshift. To study the evolved galaxy population at  $z > 3$  in order to address these questions requires deeper measurements in the  $K$ -band, over wider fields-of-view, to both better sample the population of old galaxies to lower mass, and to overcome cosmic variance in the fields. At temperate-latitude observatories the rising thermal background limits the achievable sensitivity, requiring a much larger aperture. However, from the Antarctic plateau, the extreme cold dramatically lowers the thermal background, leading to greatly improved sensitivities for the same-sized telescope.

### 3.1.2 PILOT Deep Fields

We now consider the performance possible for a  $K_d$  deep field obtained from Antarctica, compared with deep fields possible from mid-latitude locations. We have applied the Bouwens Universe Construction Set (BUCS; Bouwens et al. 2005) software package in order to generate simulated deep galaxy fields. BUCS makes use of real galaxy templates extracted from deep multi-colour HST observations, including the GOODS (Great Observatories Origins Deep Survey) field. It places these templates on the simulated frames with the same surface densities as found in the input samples. In creating the output images, shown in Figure 6, BUCS recalculates the appearance of each galaxy using the best-fit pixel-by-pixel spectral energy distributions, and then resamples this onto the output frame. The results are then smoothed to the point-spread-function (PSF) of the output image, and noise is added to reproduce the specified background noise level. By preserving both the surface densities and the pixel-by-pixel morphological details of each input object, BUCS is able to produce model-independent representations of each simulated field.

We compare the parameters of several current surveys in Table 1. The number density of galaxies to a given magnitude limit, as predicted by the models, is also listed in Table 1. PILOT could, for instance, go 1 magnitude fainter than the VLT-FIRES survey over a 3 orders of magnitude larger area, or 2 magnitudes deeper than the UKIRT-UDS over twice the area, detecting an order of magnitude more galaxies. In both cases the spatial resolution would be 2–3 times better.

The mass limits reached by a particular survey are also listed in Table 1. While obviously this limit depends on many assumptions about the stellar light of a galaxy and its evolutionary state, we make use of the work of van Dokkum et al. (2006) to list an indicative mass limit for which a particular survey will be complete, in the redshift range  $2 < z < 3$ . For  $z < 1$  the limiting mass will be less than 10 times smaller, whereas for  $z > 4$  it would be about 3 times larger. To provide a comparison between surveys, MUSYC reached to  $10^{11} M_{\odot}$  masses, while FIRES reached an order of magnitude lower in mass, but with an order of magnitude smaller field size. PILOT could reach to  $\sim 3 \times 10^9 M_{\odot}$  over a 1–3 orders of magnitude larger field size than these other surveys.

An alternative performance metric is to consider how large an area might be surveyed to a “deep” limit, as opposed to an “ultradeep” limit, in comparison to the wide-field UKIRT-DXS (Deep eXtragalactic Survey). This latter survey with the UKIRT will cover 35 deg<sup>2</sup> of sky, to a 5  $\sigma$  detection limit of  $m_{AB} = 23.0$  mags (2 mags shallower than the UKIRT-UDS). It is slated to take 118 nights of telescope time, in comparison to 296 nights for the UDS. With PILOT, integrating for 1 hour per field, the 5  $\sigma$  detection limit would be  $m_{AB} = 25.3$  mags, and 20 deg<sup>2</sup> could be covered in  $\sim 100$  nights (assuming, as does UKIRT, 10 hours of observing per night with an efficiency of 70%). As well as going 2.3 magnitudes deeper than the UKIRT-DXS over a comparable area, such a PILOT-



Table 1: Comparison of survey capabilities in  $K$ -band.

Telescope	Diam (m)	FWHM (arcsec)	Pixel Size (arcsec)	Sensitivity ( $m_{AB}$ )	Survey Area (arcmin <sup>2</sup> )	No. gal. arcmin <sup>-2</sup>	Mass Limit ( $M_{\odot}$ )
PILOT <sup>a</sup>	2.5	0.3	0.15	26.8	5000	190	$3 \times 10^9$
UKIRT <sup>b</sup>	3.8	0.8	0.40	25.0	2800	65	$2 \times 10^{10}$
Blanco <sup>c</sup>	4.0	1.2	0.31	23.0	400	20	$1 \times 10^{11}$
VLT <sup>d</sup>	8.2	0.5	0.15	25.7	6	100	$8 \times 10^9$
HST <sup>e</sup>	2.4	0.2	0.08	23.1	1	20	$1 \times 10^{11}$

<sup>a</sup> For a PILOT deep field survey with the PNIRC camera using 15 hour integrations per field, spread over 1000 hours of total observing time, with 70% observing efficiency.

<sup>b</sup> For the planned Ultra Deep Survey (UDS) using  $\sim 300$  nights observing on the UKIRT telescope as part of the UKIDSS Survey (Lawrence et al. 2007).

<sup>c</sup> From the Multi-wavelength Survey by Yale-Chile (MUSYC) on the CTIO Blanco telescope (Quadri et al. 2007).

<sup>d</sup> From the Faint Infrared Extragalactic Survey (FIRES) on the VLT telescope (Labbe et al. 2003).

<sup>e</sup> From the Hubble Deep Field South survey using the near-infrared camera and multi-object spectrograph (NICMOS) on the HST (Yahata et al. 2000).

DXS would yield an image resolution of  $0.3''$  compared to  $0.8''$ . Such wide areal coverage is also well beyond what could be covered by any survey conducted using JWST, although, of course, JWST will go much deeper ( $m_{AB} \approx 30$  at  $K$ -band) than any proposed ground-based telescope could ever achieve.

### 3.1.3 The First Stellar Populations

The discovery of galaxies at redshift  $z > 6$  with well-developed Balmer breaks (Eyles et al. 2005) is a challenge to galaxy formation theories, since these breaks take more than 200 Myr to form, and the Universe was only 1000 Myr old at that time. In any case, these must be the galaxies whose light reionised the Universe at  $z > 10$ . There is an obvious case to (a) determine the space density of these galaxies at  $z = 6$ ; (b) measure the decline rate in star forming galaxies over the range  $3 < z < 6$ ; and (c) find the very earliest stellar populations in the Universe. The galaxies found by Eyles et al. (2005) were only detected because they also have Lyman breaks (and hence ongoing star formation); it is a puzzle as to why such a large fraction (40%) of these Lyman break galaxies also have Balmer breaks. In the nearby Universe, galaxies exist with recently formed Balmer breaks but no current star formation (E+A galaxies), so we need a method that can find all Balmer break galaxies at these redshifts without depending on star formation.

Figure 7 shows the data for one of the Eyles et al. (2005) galaxies. The Spitzer data at  $4.5$  and  $3.6 \mu\text{m}$  are very good. The data at  $1.6 \mu\text{m}$  and shorter, from HST, are also good. The glaring problem is the  $K$ -band data that are essential for determining the break amplitude and hence the age and metallicity; these data have poor  $SNR$  despite representing 4–5 hours integration, in the best conditions, on an 8 m telescope. While the large breaks have been attributed to Balmer breaks,

it is possible that emission lines in the Spitzer bands could also be responsible.

The Spitzer warm mission is now funded for at least two years; the Infrared Array Camera (IRAC) will continue to work as before in its two shortest bands. It happens that, for this project, the IRAC sensitivities are almost perfectly matched to those of PILOT at  $K_d$ . IRAC reaches  $0.5 \mu\text{Jy}$  in 1 hour at  $3.6 \mu\text{m}$  and  $0.5 \mu\text{Jy}$  in 4 hours at  $4.5 \mu\text{m}$ . The expected [ $K_d - 3.6 \mu\text{m}$ ] flux ratio is a factor 3–4 (e.g., van Dokkum et al. 2007). PILOT+PNIRC (with a field 5 times larger) will take 4 hours to reach the required  $0.15 \mu\text{Jy}$  at  $K_d$ . PILOT can thus provide matching  $K_d$  photometry (and accurate positions) for essentially all IRAC detections, in similar timescales. The spectral signal is very distinct—a 1.5 mag jump and then flat.

The redshift range over which we could detect galaxies by this method corresponds to when the Balmer break is between the  $K_d$  and  $3.6 \mu\text{m}$  bands, i.e.,  $z = 5-7$ . Note that Mobasher et al. (2005) claim sources at  $z \approx 6.5$ , but this is disputed (Muñoz & Loeb 2008). PILOT also provides a window for detecting galaxies with the break between the  $3.6 \mu\text{m}$  and  $4.5 \mu\text{m}$  bands (as  $3.6 \mu\text{m}$  dropouts) at a redshift  $z = 9-11.5$ . Such galaxies are not thought to exist, but this needs to be demonstrated.

Eyles et al. (2005) detected 6 galaxies with  $z \approx 6$  in an area of  $150 \text{ arcmin}^2$ . The number of galaxies that are undetected because they have no star formation is unknown. To determine a luminosity function, and understand the evolution of the population, requires several hundred to be found at least, necessitating a survey of a few square degrees. Such a survey would take  $\sim 500$  hours with PILOT.

For PILOT, the science payoff is obvious. All that is needed is for Spitzer to undertake some of its major extragalactic surveys far enough south to be observable by PILOT. For Spitzer, which will probably be

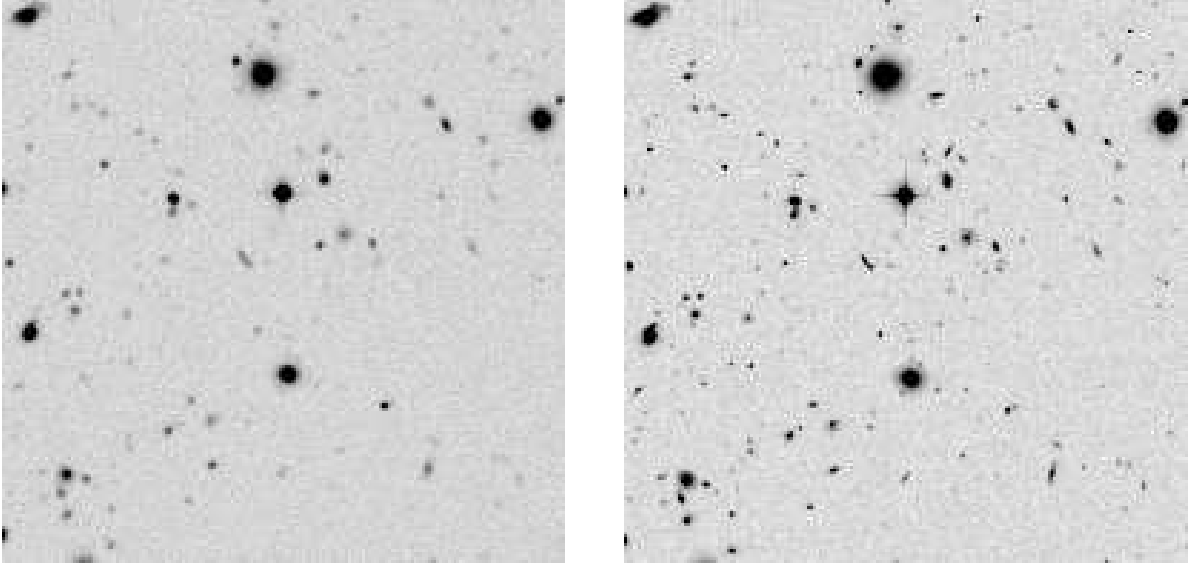


Figure 6: Left: Simulated ultra-deep  $K$ -band image, calculated using BUCS, as could be obtained by the UKIRT-UDS, achieving a  $5\sigma$  galaxy detection limit of  $m_{AB} = 25.0$ . A  $30' \times 30'$  field is shown, with spatial resolution  $0.8''$ . Right: A similar simulation for a  $K_d$  image, as could be obtained by PILOT in 15 hours of integration, achieving a  $5\sigma$  galaxy detection limit of  $m_{AB} = 26.8$ . The same field is shown, with a spatial resolution of  $0.3''$ . Roughly 200 galaxies per arcmin<sup>2</sup>, three times as many as the UKIRT-UDS, are detected. The complete PILOT survey could cover  $\sim 5000$  arcmin<sup>2</sup> at this depth.

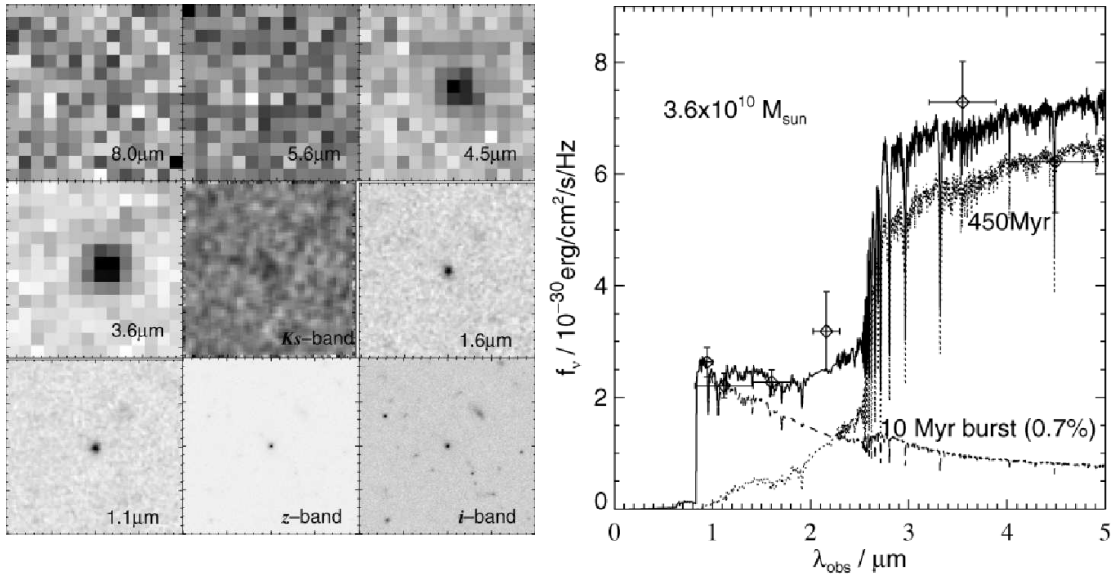


Figure 7: Left: postage-stamp images (each  $8''$  across) at different wavebands of a spectroscopically confirmed  $z = 5.83$  Balmer break galaxy. Data comes from HST-ACS ( $i$ - and  $z$ -band), HST-NICMOS ( $J$ - and  $H$ -band), VLT-ISAAC ( $K$ -band) and Spitzer-IRAC ( $3.6$ – $8\ \mu\text{m}$ ). Right: best fit synthetic spectrum, combining star forming and 450 Myr populations. From Eyles et al. (2005).

decommissioned before PILOT is built, the payoff is less immediate. However, the existence of BLANCO Dark Energy Survey (DES)  $g$ ,  $r$ ,  $i$ ,  $z$  photometry, and the proximity of the South Ecliptic Pole (which is just

outside the DES area) provides an argument to choose a suitable area now.

## 3.2 Witnessing Galaxy Cluster Assembly at Moderate Redshift

### 3.2.1 Impact

The field of galaxy cluster studies has entered a renaissance with modern data sets such as 2dFGRS and SDSS being made publicly available. There are thousands of clusters now catalogued, each with tens (if not hundreds) of associated galaxies with photometric and spectroscopic data readily available for download. These datasets have allowed us to gain an unprecedented picture of how galaxy clusters grow through the accretion of smaller groups of galaxies as they fall into the cluster potential anisotropically along filaments. Indeed, to pick just one example from many, we now know that there is a critical density (or clustercentric radius) for galaxy formation (e.g., Gómez et al. 2003; Lewis et al. 2002). However, it is worth noting that the median redshift for the SDSS and 2dFGRS surveys is still low: in the region of  $0.10 < z < 0.15$ . The relatively smaller amount of data that we have on significantly higher-redshift clusters comes usually from only the most massive clusters (since they are easier to detect, e.g., at X-ray wavelengths) and have typically not been surveyed in a systematic wide-field manner.

There are therefore two obvious gaps in our dataset: the existence of a long redshift baseline to delineate the effects of cosmic time on the galaxy populations of clusters, and a range in the mass of galaxy clusters at different epochs to delineate the role of environment.

Here, we propose a suite of observations to observe high-redshift clusters and their environment in a homogeneous manner. We will be surveying the field regions and filament regions that are fuelling the cluster growth.

So called third-generation X-ray surveys such as the XMM distant clusters project have generated thousands of possible detections of  $z > 0.5$  galaxy clusters (e.g., Fassbender 2008). Observations of this high-redshift sample would provide a large redshift baseline and some degree of mass range at high redshift to compare with our lower-redshift cluster samples (see e.g., Stott et al. 2007). This would yield important information in a number of areas, including, but not limited to:

- the evolution and build-up of the colour magnitude relation with redshift, including how elliptical and lenticular galaxies form and evolve; this would also test the monolithic collapse scenario versus the assumed hierarchical assembly model. We should be seeing a large amount of scatter in high-redshift colour-magnitude diagrams during the peak epoch of star formation at  $z \approx 1$ ,
- the role of AGN feedback over a large epoch in look-back time,
- the formation epoch and subsequent evolution of brightest cluster (cD class) galaxies and how they relate to their local environment,
- the amount of recent major cluster-cluster merging activity to test predictions from modern semi-analytic simulations (e.g., the Millennium run),
- the morphology-density-star formation-colour relationships at high redshift (cf., Smith et al. 2005), and hence the relationship to the Butcher-Oemler effect,
- quantification of the effect of downsizing (i.e., star-formation occurring in smaller mass galaxies with decreasing redshift) out to large redshift (cf., Cucciati et al. 2006) and, as illustrated in Figure 8, the lack of faint red galaxies at this high-redshift epoch (Stott et al. 2007; De Lucia et al. 2004), and
- the role of the cluster environment within a supercluster context (Stott et al. 2007, 2008).

### 3.2.2 Other Facilities

Most previous observations of high-redshift clusters have taken place in a limited context. The number of clusters studied has been small, and hence real local cluster-to-cluster variations can dominate the ensemble. The field-of-view has been moderately small (meaning that only the central Mpc or less might be viewed—especially true of HST where complex tessellation patterns are required to map out clusters to significantly large radii) thereby denying us a view of the filaments and infalling groups that will come to accrete on to the cluster potential in the next few Gyr and the location of a given cluster within a supercluster environment. Finally, the resolution of existing surveys is poor, such that individual galaxy morphologies may only be crudely estimated.

PILOT offers a unique blend of a large field-of-view, allowing us to probe to significant radii and density regimes in an homogeneous manner; an excellent resolution, important for morphological dissection; and excellent prospects of obtaining a large amount of data across the southern sky without having to wait for the telescope to re-visit a given pointing several times in order to build up good photometry.

### 3.2.3 Observations

We note from the outset that cluster and supercluster observations could readily “piggy-back” on other potential science drivers and could therefore represent an excellent return on investment. To perform the kind of science outlined here, we need to observe sufficiently far down the luminosity function to effectively probe the fainter galaxies where much of the star formation would be likely to occur— $M^* + 2$  would be about ideal in the first instance to determine the population, or lack thereof, of faint red colour-magnitude ridge-line objects. Ideally, we require wide-field observations made in a homogeneous manner, preferably in photometric conditions. At low redshifts, several authors have made progress by actively pursuing galaxy evolution to very large clustercentric radii (Wake et al. 2005; Pimblet et al. 2006)—certainly out to  $\sim 8$  Mpc. At high redshifts (say  $0.8 < z < 1.5$ ), the distance scale would be as much as 8 kpc per arcsec meaning that the distance on the sky would be much less than a degree for matching to baseline  $z \approx 0.1$  observations. An  $M^*$  galaxy at  $z = 0.8$  corresponds roughly to  $m_{AB} = 24.5$

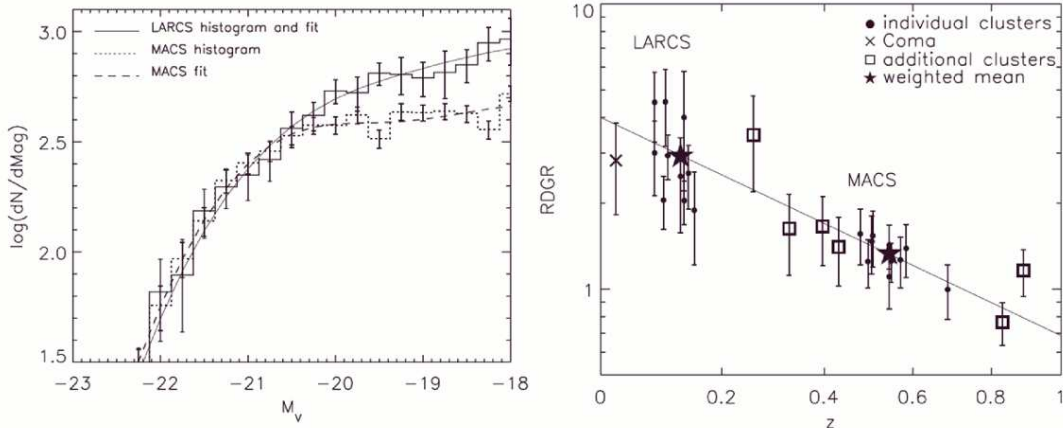


Figure 8: Left: luminosity functions for red-sequence galaxies in low (LARCS) and high (MACS) redshift samples demonstrating faint red galaxy excess. Right: variation in Red-sequence Dwarf to Giant Ratio (RDGR) in clusters versus redshift. From Stott et al. (2007).

at  $V$ -band (or  $m_{AB} = 25.5$  by  $z = 1.0$ ). According to Romer et al. (2001) and Fassbender (2008) there are about 750 clusters at  $z < 0.6$  and perhaps up to 100 more in the range  $0.6 < z < 1.5$  identifiable from the XMM cluster survey.

A proposed project for PILOT is to image a sample of 100 galaxy clusters in the range  $0.6 < z < 1.5$ . This is a large enough sample to be homogeneous enough to beat down the local cluster variations. The image size of the PILOT wide field visible camera, PVISC, is large enough that the majority of clusters can be observed with a single pointing. Three bands in the visible ( $r$ ,  $i$ , and  $z$ ) would be chosen to straddle the 4000 Å break at these redshifts, and to give a comfortable dynamic range to derive colours. The expected sensitivities of PVISC implies  $\sim 1$  hour of observation per filter per cluster. The complete survey would thus take  $\sim 300$  hours. Ideally, follow-up observations of the same clusters in the near-infrared  $J$ ,  $H$ , or  $K$ -bands with the PNIRC camera would give an even larger dynamic baseline. For such a small investment in observing time, this project should represent the largest sample of X-ray selected clusters examined at these redshifts.

## 4 Dark Matter and Dark Energy

### 4.1 Weak Lensing

#### 4.1.1 Overview

Cosmic shear offers a relatively clean way to measure the evolution of the power spectrum, and hence the equation of state, of the Universe. The observations are in principle simple: since large-scale structure has a quadrupolar lensing effect on background galaxies, we can map this structure by measuring the shapes of

faint galaxies. Large numbers ( $\sim 10^9$ ) are needed, to extract the faint lensing signal from the much larger intrinsic shape variation, and to overcome cosmic variance. If we know the approximate distances for these faint galaxies, and can measure the lensing for separate distance classes, then we can measure the evolution of clustering, which in turn depends directly on the equation of state. The measurement is clean because we measure mass fluctuations in the linear regime. Weak lensing has been recognised as the most promising route for determining the characteristics of dark energy by NASA, NSF and ESA.

Because of its importance, a large number of weak-lensing surveys are currently planned. From the ground there is: the Dark Energy Survey (2009), KIDS on VST (2009), HyperSuprimeCam on Subaru ( $\sim 2010$ ), PanSTARRS-4 ( $\sim 2012$ ), and LSST ( $\sim 2014$ ). From space there is DUNE (now part of EUCLID;  $\sim 2018$ ), and JDEM/SNAP ( $\sim 2018$ ). For PILOT to make an impact, it must be better than any of the ground-based surveys, and faster (or better) than the space missions.

#### 4.1.2 Why Antarctica?

The intrinsic effects of lensing are  $\sim 1\%$  changes in ellipticity. The galaxies at the required distances and surface densities have  $m_{AB} \approx 26$  and are smaller than the best existing ground-based seeing (Figure 9). Seeing dilutes the lensing signal by the square of the overall observed image size. This translated directly into both the signal-to-noise required per galaxy, and the sensitivity to systematic error in the PSF. It also increases the sky noise, to give an overall integration time per source varying as the sixth power of the observed image size (Kaiser et al. 2000). The overall survey speed (assuming the pixels are a fixed fraction of the seeing) varies as the fourth power of the observed image size. For  $0.3''$  FWHM galaxies, this translates to an order of magnitude gain for Dome C over temperate

Table 2: Parameters for large lensing surveys.

Telescope/ Instrument	Diam (m)	Giga- pixels	Res. <sup>a</sup> (arcsec)	Signal <sup>b</sup>	Survey speed <sup>c</sup>	Year <sup>d</sup>
MegaCam	3.6	0.34	0.7	0.16	0.11	2003
VST	2.6	0.28	0.8	0.12	0.03	2009
DES	4	0.5	0.9	0.10	0.08	2009
PanSTARRS	1.8	1.4	0.6	0.20	0.18	2009
PanSTARRS-4	3.6	1.4	0.6	0.20	0.73	2012
<b>PILOT</b>	<b>2.5</b>	<b>1.0</b>	<b>0.2<sup>e</sup></b>	<b>0.69</b>	<b>3.00</b>	<b>2013</b>
HyperSupCam	8.2	1	0.7	0.16	1.62	2013
LSST	6.5	3	0.7	0.16	3.05	2014
DUNE	1.2	0.65	0.23	0.63	3.71	2018
SNAP	1.8	0.45	0.15	0.80	9.33	2018

<sup>a</sup>Resolution is the FWHM image quality determined by the atmospheric seeing conditions, the telescope correction system, or the diffraction limit.

<sup>b</sup>Signal is the dilution of the lensing signal for a 0.3'' FWHM galaxy.

<sup>c</sup>Survey speed is the relatively time to complete a survey of a given area to a given depth.

<sup>d</sup>Year is the planned date that the survey will begin.

<sup>e</sup>The PILOT project is undertaken in the 50% best Dome C seeing conditions.

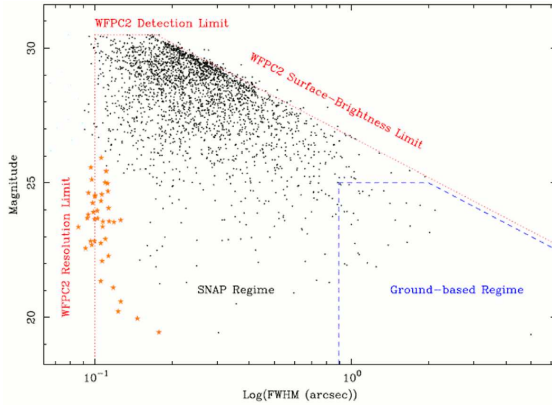


Figure 9: Image size for galaxies from the HDF, as a function of AB magnitudes. From Curtis et al. (2000).

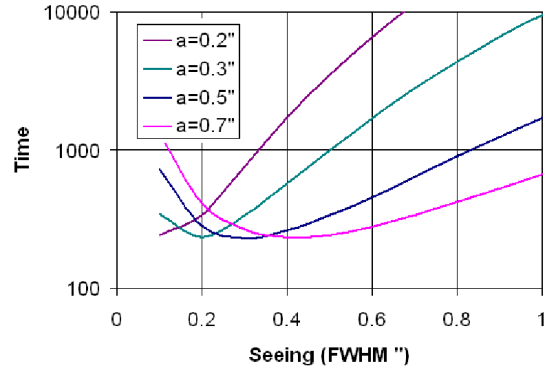


Figure 10: Overall weak-lensing survey speed as a function of seeing for galaxies of size 0.2, 0.3, 0.5, and 0.7'', assuming that the detector pixels are a fixed fraction of the seeing.

sites (as shown in Figure 10), making PILOT competitive in survey speed with wide-field 8 m class telescopes such as HyperSuprimeCam or LSST (see Table 2).

However, an even more serious limitation for temperate sites comes from the PSF stability. Systematic effects in the variation of the PSF (with time, colour, and field position) must be understood and modelled at a level better than the diluted lensing signal. The net effect is that even with 8 m telescopes “data collected in seeing worse than 0.8'' is of little use for weak lensing” (Kasliwal et al. 2008). In practice, the combined effects of sensitivity and systematics limit the size of galaxies to be comparable with the seeing, giving a surface density at temperate

sites of 10–20 galaxies/arcmin<sup>2</sup>, compared with 50–100 galaxies/arcmin<sup>2</sup> from space (e.g., Kasliwal et al. 2008).

At Dome C, the lensing signal is several times stronger (Table 2). Moreover, the better seeing means slower telescope and camera optics, which means excellent image quality is much more readily achieved and maintained over wide focal planes. It is safe to assume we can control PSF systematics to the same level, in pixels, as temperate telescopes. This allows us to reach a surface density  $\sim 3$  times higher, and a median depth  $\sim 50\%$  greater. This increases (a) the sensitivity to lensing, (b) the volume surveyed, and (c) the redshift lever-arm for measuring the evolution of the power

spectrum.

### 4.1.3 PILOT Parameters

We assume a PanSTARRS-type Orthogonal Transfer Array camera with 1.4 Giga-pixels. A camera with traditional CCD's (e.g.,  $10 \times$  STA1600A detectors, 1.1 Giga-pixels) would be somewhat less efficient, but would have better PSF constancy (because there are no anisoplanatic guiding errors). Which of these is the optimal detector technology for a weak-lensing survey has not yet been determined.

Either way, PILOT would reach  $SNR = 10$  for  $m_{AB} = 25.6$  for  $0.3''$  FWHM galaxies, with an optimised  $r+i+z$  filter in 30 minutes. This gives  $\sim 40$  galaxies per arcmin<sup>2</sup>, which allows measurement of the peak of the lensing power spectrum at  $l \approx 5000\text{--}10\,000$  ( $2\text{--}4'$  scales). This scale is where the greatest sensitivity to cosmological models occurs.

Determining the evolution of the power spectrum requires photometric-redshift determination. It would not be an efficient use of PILOT time to undertake the required photometry. However, the Dark Energy Survey (DES; Annis et al. 2005) will obtain  $g, r, i, z$  photometry to limits of  $m_{AB} = 26.1, 25.6, 25.8, 25.4$ , respectively, for  $4000 \text{ deg}^2$  with  $\delta < -30$ ; this is essentially all the high-latitude sky available to PILOT. This region of sky will be surveyed at millimetre wavelengths by the South Pole Telescope (SPT). It will also be covered by the VISTA VHS survey in the infrared, but not deeply enough to be useful. This limits the maximum redshift to  $z \approx 1.2$  (as the Balmer break moves into the  $z$ -band).

### 4.1.4 Proposed Survey

The proposed project for PILOT is to survey the  $4000 \text{ deg}^2$  DES/SPT area, to a depth giving  $10 \sigma$  detections of the galaxies at the  $5 \sigma$  DES limit ( $m_{AB} \approx 25.6$ ). Because the speed of such a survey depends so dramatically on image quality, we propose that this survey only be undertaken in better than median seeing conditions, and in dark or grey time. The required integration time is about 30 minutes per field, and the time to cover the entire DES/SPT area is 2500 hours, or a third of the available time over 4 years.

Compared with the proposed DUNE space mission (now part of EUCLID, proposed for 2018), a PILOT lensing survey looks remarkably good. The overall survey speeds, taking into account the image quality, sky background, aperture, and field-of-view, are about the same. PILOT can only access  $\sim 25\%$  of the high Galactic latitude sky, and PILOT will not be capable of obtaining the deep  $Y, J,$  and  $H$ -band data proposed for DUNE. However, this does not affect the main weak-lensing science goals. The constraints on the equation of state for DUNE are shown in Figure 11. Because the PILOT survey has a smaller area, the error ellipses are a factor 2 larger. They are still much better than those calculated for, e.g., LSST (Tyson et al. 2006).

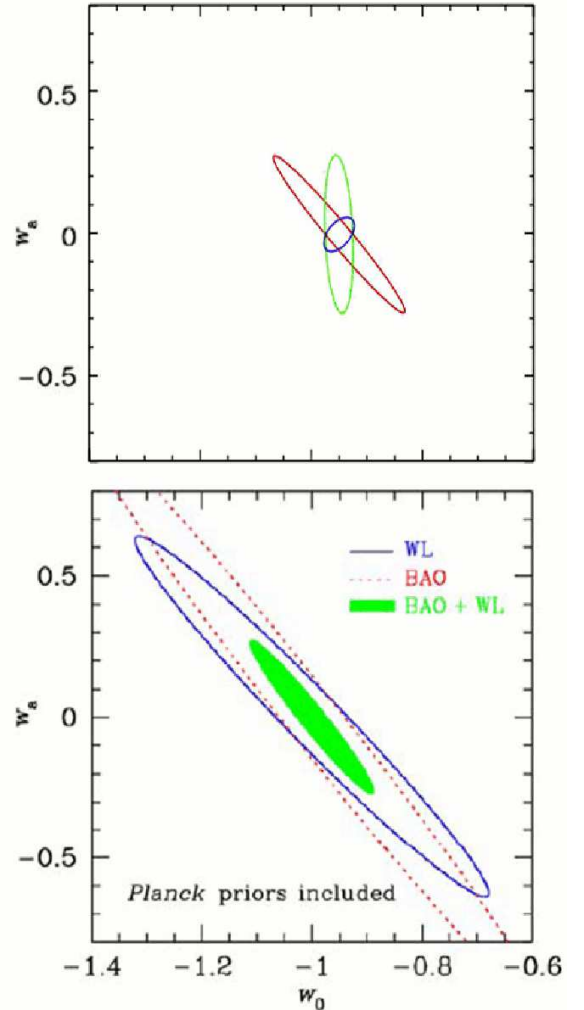


Figure 11: Top: constraints on cosmological parameters measured from the DUNE weak-lensing survey. Different coloured contours correspond to different assumptions for the photometric redshift errors and for the pivot point  $a_n$ . From Refregier et al. (2006). The PILOT errors would be a factor of two larger than the red or green ellipses. Bottom: constraints from the LSST survey. Contours are constraints from baryon acoustic oscillations (BAO) and weak lensing (WL). The shaded region combines the two. From Tyson et al. (2006). In both plots,  $\omega$  is parameterised as  $\omega(a) = \omega_n + (a_n - a)\omega_a$ .

## 4.2 Dusty Supernovae

### 4.2.1 Impact

Supernovae (SNe) are at the intersection of cosmology, galaxy evolution, and stellar evolution. SNe are studied as the end product of the evolution of massive stars via core collapse. They eject most of their external layers into the interstellar medium (e.g., Arnett et al.

1989), and they might be the major dust factory in the Universe through condensation of dust grains in their ejecta (e.g., Nozawa et al. 2003). Dust formation in SNe may play a major role in the evolution of galaxies since the dust absorbs and scatters ultraviolet photons in the far-infrared. Finally, SNe (Type Ia) are standard candles via which the cosmic acceleration of the Universe can be probed (e.g., Schmidt et al. 1998; Perlmutter et al. 1999). This last point is the main driver for PILOT supernovae studies.

The use of SNe is strongly constrained by the environment in which they explode. If these very violent events appear in a dusty environment, there are likely to be uncertainties introduced in the estimation of their distance and absolute brightness from their optical light curve. This necessarily leads to errors in the derived Hubble diagram. As discussed by Burgarella et al. (2008), the dust attenuation in magnitudes at  $K$  is only one-ninth of that at  $V$  (Rieke & Lebofsky 1985). This is illustrated by recent results showing that some supernovae (e.g., SN 2002cv) that are not detected in optical surveys are easily detected in the infrared (Di Paola et al. 2002). The  $V$ -band non-detection suggests that there is a large variation in the dust attenuation of observed supernovae. This is supported by Maiolino et al. (2002) who estimate that the  $V$ -band dust attenuation of SN2001db was  $\sim 5$  magnitudes higher than the average dust attenuation for a more usual sample of supernovae. Astier et al. (2006) stated that “there is no consensus on how to correct for host galaxy extinction affecting high-redshift SNe Ia”.

Observing in the infrared should allow more accurate interpretation of SN light curves by negating dust effects, and hence obtaining more accurate constraints on the cosmological parameters derived from SN Ia distance relationships. Recent results have confirmed that for nearby supernovae, with redshifts up to  $z = 0.1$ , near-infrared light curves are excellent standard candles, even without correction for reddening (Wood-Vasey et al. 2007; Krisciunas et al. 2004a). It has been suggested that specific wavelengths and redshifts occur that allow a much higher precision distance indicator due to small  $K$ -corrections; for example, where the  $J$ -band rest-frame is shifted to  $K$ -band at  $z = 0.73$  (Krisciunas et al. 2004b). An additional advantage of the infrared for supernovae searches is that, as shown in Figure 12, the light curves are flatter for a longer time than in the visible (Krisciunas et al. 2003; Di Carlo 2004). This means there is a longer opportunity to detect these supernovae than in the optical and that the signal-to-noise ratio will be higher for a longer period. Additionally, with a high angular resolution it should be possible, with PILOT, to detect supernovae in the nuclear regions of galaxies where source crowding makes detection with Spitzer, for example, difficult (Chary et al. 2005).

While cosmological studies from SN Ia provide the prime motivation for PILOT supernovae searches, the study of supernovae environments would also be enabled by such a search. The study of dust and dust-related phenomena are important for our understanding of star formation in the Universe, and in evaluating the star formation rate of SN host galaxies (for core-

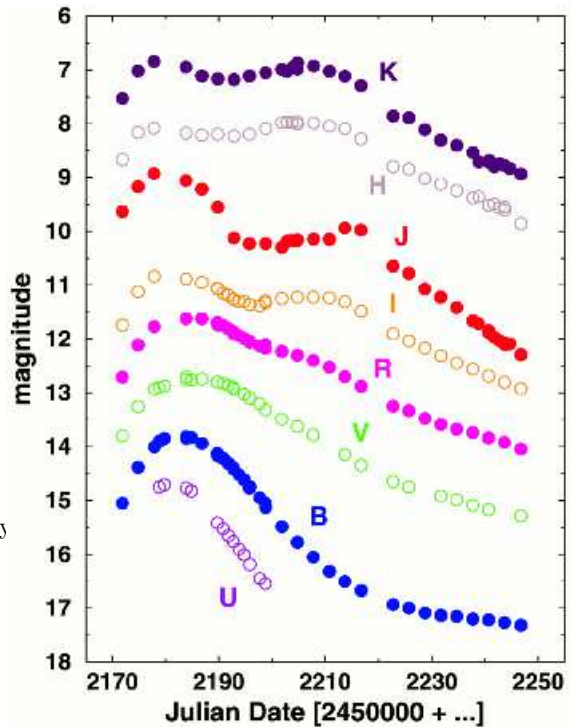


Figure 12: Optical and infrared light curves of SN 2001el. Bands have been offset for plotting purposes. From Krisciunas et al. (2003). These data show that the peak brightness occurs earlier in the infrared bands than in the visible, but that the infrared light curves are flatter for a longer period after reaching maximum.

collapse SNe). We know that most of the star formation in the Universe at  $z \approx 1$  is hidden in dust (e.g., Takeuchi et al. 2005); even ultraviolet selected galaxies such as Lyman Break Galaxies can present a large dust emission and appear as Luminous Infrared Galaxies with  $10^{11} < L_{dust}/L_{\odot} < 10^{12}$  (Burgarella et al. 2007). The detection of supernovae in dusty environments is therefore a very promising way to explore the relationship between SN processes and the environment in which they occur (e.g., Chary et al. 2005; Pozzo et al. 2006; Elias-Rosa et al. 2006).

#### 4.2.2 PILOT Observations

Figure 12 shows that SNe stay close to the maximum of light (i.e.,  $\pm 0.25$  mag) for about 20 days. The SN detection limits for PILOT as a function of redshift within this timeframe are shown in Figure 13 for  $J$ -band and  $K$ -band observations. This plot shows that the optimum near-infrared wavelength to search for relatively high-redshift ( $z > 1$ ) SNe is  $J$ -band. A 1 hour exposure at  $J$ -band should detect (at  $5\sigma$ ) SN Ia out to a redshift of  $z \approx 1.4$ . Based on the cumulative distribution surface density of SN Ia shown in Figure 14, a dedicated  $J$ -band search with PNIRC

monitoring a  $\sim 6 \text{ deg}^2$  region (200 fields) of sky with 1 hour exposures and a 10 day cadence would yield  $\sim 100$  SN Ia in the range  $0.6 < z < 1.0$ , and  $\sim 200$  SN Ia in the range  $1.0 < z < 1.4$  per season. The majority of these SNe could be followed-up in  $H$ - and  $K$ -bands with  $\sim 4$  hour exposures, resulting in only a small reduction in the total expected number of detections. Longer exposures at  $L$ - and  $M$ -bands could also be obtained for a subset of these SN.

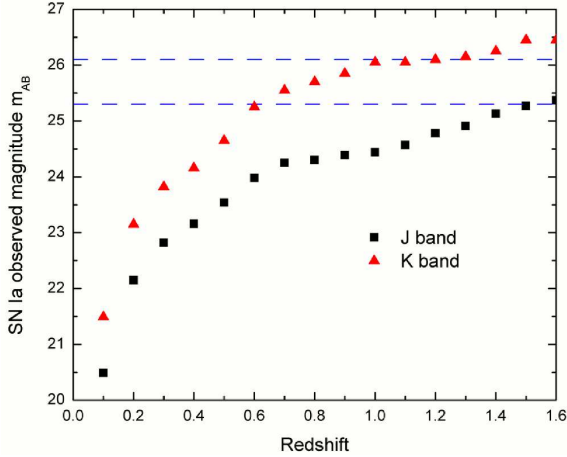


Figure 13: The black square data points show the  $J$ -band observed magnitude within 10 days of peak brightness for Type Ia supernovae as a function of redshift given by Tonry et al. (2003). The red triangular data points show an estimate of the  $K$ -band observed magnitude based on extrapolations of the Tonry et al. (2003) data using the infrared rest-frame absolute peak brightness given by Krisciunas et al. (2004b). The horizontal dashed lines show the PILOT PNIRC detection limit for 1 hour and 4 hour integrations at  $K_d$ -band. The  $J$ -band detection limit is 0.3 magnitudes fainter.

While such a dedicated project would yield a significant number of SN Type Ia infrared light curves, similar detection rates should be possible with, for example, VISTA operating at  $J$ -band. The sensitivity of VISTA at longer wavelengths, however, is not high enough to allow follow-up of large numbers of detections at  $H$  and  $K$ . In principle, the longer wavelength follow-up could be achieved on an 8 m class telescope with an adaptive optics system, although this still represents a large observing program for such a telescope (i.e., several thousand hours).

As opposed to a dedicated search program, a more efficient use of observing time would be to utilise the data collected from other proposed PILOT wide-field infrared survey projects. For example, the PISN search (Section 2.1) and the high-redshift galaxy survey (Section 3.1) will both observe large regions of the sky at  $K_d$ . With an appropriate cadence these searches would be expected to find, for example,  $\sim 60$  SN Ia per season out to  $z \approx 0.6$  for a shallow survey of

$m_{AB} = 25.3$  per field, or  $\sim 60$  SN Ia per season in the range  $1.0 < z < 1.6$  for a deeper survey to a depth of  $m_{AB} = 26.7$  per field. Additionally, the weak-lensing survey in the optical will cover a very wide region of sky ( $\sim 4000 \text{ deg}^2$ ). If this survey were built up from a series of shallow repeat visits, thousands of low-redshift ( $z < 0.5$ ) SN Ia would be discovered. SNe detected via any of these survey projects should be followed up throughout the near-infrared with the PNIRC instrument. In addition to Type Ia supernovae, core collapse supernovae would also be found in such searches. The brightness of CC SN is typically 2–3 magnitudes fainter than Type Ia SN (e.g., Hamuy 2003), and thus they would be difficult to detect at high redshifts. However, they occur in much greater number densities, as shown in Figure 14, and thus should be detectable in large numbers at redshifts below  $z \approx 0.2$ .

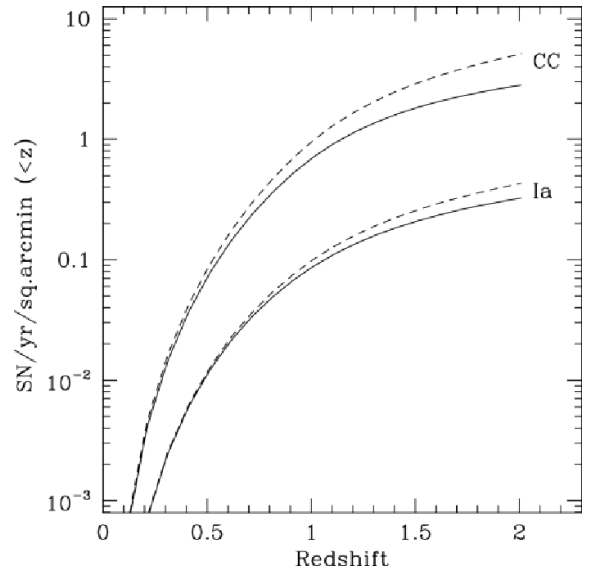


Figure 14: Predicted cumulative number of core collapse (CC) and Ia SNa as a function of redshift. From Manucci et al. (2007).

The SN project proposed here takes advantage of the wide field-of-view, good temporal coverage, high angular resolution, and high infrared sensitivity of the PILOT telescope. These characteristics provide a unique opportunity to build an unbiased sample of infrared light curves of SN Ia up to a redshift of about  $z \approx 1.4$ . While there are several current supernovae search programs, e.g., the Canada-France-Hawaii Telescope Legacy Survey project (Astier et al. 2006), these are primarily devoted to finding large numbers of SNe with multi-colour optical photometry. With a dedicated search program, PILOT can play an important role in removing (or confirming) concerns that dust may affect the validity or uncertainty of current constraints placed on cosmological parameters based on optical data. In addition, the PILOT sample of SN Ia will form a subset of the thousands of high-redshift infrared detections possible with the proposed SNAP mission.



This will thus be an important precursor experiment allowing the refinement of experimental techniques and the control and understanding of systematic effects.

## 5 Conclusion

The detection and characterisation of the signatures of the first stars to form in the Universe is observationally very challenging; the PILOT discovery space, however, is well suited to such science. With a wide-field high-sensitivity near-infrared camera, PILOT is likely to be one of only two facilities (the other being JWST) capable of detecting statistically significance numbers of pair-instability supernovae at high redshift. These objects should provide a rare view of the physical conditions in the early Universe. No confirmed detection of such an object has yet been made, however, and there are large uncertainties as to their expected characteristics. The observational parameter space explored by PILOT and JWST are generally quite distinct, allowing separate regions of the potential parameter space (i.e., the expected brightness and rarity) for PISN to be examined. The high sensitivity in the thermal infrared and the large wavelength coverage of the PILOT infrared instrument suite, combined with the potential for high cadence observations, are ideally matched to a search for high-redshift gamma-ray burst afterglows. A dedicated program of high-energy satellite-alert follow-up would be expected to find a number of very high-redshift gamma-ray burst afterglows each season and to probe the rate of high-redshift gamma-ray burst orphan-afterglows to a lower number density than possible with any other facility.

Two projects have been proposed here that demonstrate the potential for PILOT to investigate the formation and evolution processes of distant galaxies and galaxy clusters. The first project takes advantage of PILOT's wide field-of-view and high sensitivity in the near-infrared. These factors enable deep/wide-area near-infrared surveys to be accomplished that are much deeper and have a higher spatial resolution than possible with other ground-based telescopes, and that cover a much wider area of sky than possible with space-based facilities such as JWST. Such surveys will allow the characteristics of the the earliest galaxy populations at high redshift to be explored in detail. The second project utilises the wide field-of-view and high spatial resolution of PILOT at visible wavelengths. These factors allow the assembly processes of galaxy clusters at moderate redshift to be investigated with much higher efficiency than possible with other facilities.

PILOT will be particularly capable at investigating the nature and evolution of cosmological parameters, such as dark energy and dark matter. The wide field-of-view, high spatial resolution, and stable PSF of the PILOT optical camera are requirements that are well-suited to the statistical study of weak-lensing effects on distant galaxies; a method by which the equation of state of the Universe can be investigated. For this science, PILOT is competitive in terms of survey speed and will achieve tighter constraints on cosmological parameters than the proposed LSST weak-lensing

survey, which is well ahead of the capabilities of other ground-based telescopes. PILOT is also competitive in terms of survey speed with the proposed space-based weak-lensing mission, DUNE; PILOT will not obtain the same level of constraints but its survey can be accomplished before DUNE achieves first light. Additionally, the wide field-of-view combined with a high infrared sensitivity and wide wavelength coverage of the PILOT near-infrared camera will enable it to detect and obtain infrared light-curves for larger numbers of Type Ia supernovae at higher redshift than possible with any other current facility. These data will allow tighter constraints to be placed on the expansion of the Universe by correcting for the effects of dust extinction and reddening.

## Acknowledgments

The PILOT Science Case, presented here, was produced as part of the PILOT conceptual design study, funded through the Australian Department of Education, Science, and Training through the National Collaborative Research Infrastructure Strategy (NCRIS) scheme, and the University of New South Wales through the UNSW PILOT Science Office. The European contribution has been supported by the ARENA network of the European Commission FP6 under contract RICA26150.

## References

- Abel, T., Bryan, G.L., & Norman, M.L. 2002, *Science*, 295, 93
- Agabi, A., et al. 2006, *PASP*, 118, 344
- Akelof, C., et al. 1999, *Nature*, 398, 400
- Annis, J., et al. 2005, *Dark Energy Survey White Paper*
- Arnett, W.D., Bahcall, J.N., Kirshner, R.P., & Woosley, S.E. 1989, *ARA&A*, 27, 629
- Astier, P., et al. 2006, *A&A*, 447, 31
- Band, D.L., et al. 2008, *ApJ*, 673, 1225
- Barkana, R., & Loeb, A. 2004, *ApJ*, 601, 64
- Bouwens, R.J., Illingworth, G.D., & Magee, D.K. 2005, *ASP Conf. Ser.*, 347, 100
- Bromm, V., & Larson, R. 2004, *ARA&A*, 42, 79
- Bromm, V., & Loeb, A. 2006, *ApJ*, 642, 382
- Burgarella, D., Le Floch, E., Takeuchi, T.T., Huang, J. S., Buat, V., Rieke, G.H., & Tyler, K.D. 2007, *MNRAS*, 380, 986
- Burgarella, D., Le Roux, B., Langlois, M., Moretto, G., Fusco, T., & Ferrari, M. 2008, *EAS Pub. Ser.*, 33, 147
- Burton, M.G., et al. 1994, *Proc. ASA*, 11, 127

- Burton, M.G., Storey, J.W.V. & Ashley, M.C.B. 2001, PASA, 18, 158
- Burton, M.G., et al. 2005, PASA, 22, 199
- Chary, R., Dickinson, M.E., Teplitz, H.I., Pope, A., & Ravindranath, S. 2005, ApJ, 635, 1022
- Cucciati, O., et al. 2006, A&A, 458, 39
- Curtis, D., et al. 2000, SNAP proposal to DoE and NSF
- De Lucia, G., et al. 2004, ApJL, 610, 77
- den Herder, J.W., et al. 2007, Proc. SPIE, 6688, 668805
- Di Carlo, E. 2004, Mem. Soc. Astron. Italiana, 75, 150
- Di Paola, A., et al. 2002, A&A, 393, L21
- Elias-Rosa, N., et al. 2006, MNRAS, 369, 1880
- Eyles, L.P., et al. 2005, MNRAS, 364, 443
- Fassbender, 2008, PhD thesis, Ludwig-Maximilians-Universitaet Muenchen
- Fox, D.B., et al. 2005, Nature, 437, 845
- Gardner, J.P., et al. 2006, Space Sci. Rev., 123, 485
- Gehrels, N., et al. 2004, ApJ, 611, 1005
- Gehrels, N., et al. 2005, Nature, 437, 851
- Glazebrook, K., et al. 2004, Nature, 430, 181
- Gómez, P.L., et al. 2003, ApJ, 584, 210
- Gou, L.J., Meszaros, P., Abel, T., & Zhang, B. 2004, ApJ, 604, 508
- Hamuy, M. 2003, ApJ, 582, 905
- Heger, A., & Woosley, S.E. 2002, ApJ, 567, 532
- Heger, A., Woosley, S., Baraffe, I., & Abel, T. 2002, Lighthouses of the Universe: The Most Luminous Celestial Objects and Their Use for Cosmology, ed. M. Gilfanov, R. Sunyaev, & E. Churazov, 369
- Inoue, S., Omukai, K., & Ciardi, B. 2007, MNRAS, 380, 1715
- Jakobsson, P., et al. 2005, MNRAS, 362, 245
- Kaiser, N., Tonry, J.L., & Luppino, G.A. 2000, PASP, 112, 768
- Karlsson, T., Johnson, J. L., & Bromm, V. 2008, ApJ, 679, 6
- Kasliwal, M.M., Massey, R., Ellis, R.S., Miyazaki, S., & Rhodes, J. 2008, ApJ, 684, 34
- Kawai, N., et al. 2006, Nature, 440, 184
- Kenyon, S.L., & Storey, J.W.V. 2006, PASP, 118, 489
- Kenyon, S.L., Lawrence, J.S., Ashley, M.C.B., Storey, J.W.V., Tokovinin, A., & Fossat, E. 2006, PASP, 118, 924
- Kouveliotou, C., et al. 1993, ApJL, 413, L101
- Krisciunas, K., et al. 2003, AJ, 125, 166
- Krisciunas, K., Phillips, M.M, & Suntzeff, N.B. 2004a, ApJ, 602, L81
- Krisciunas, K., et al. 2004b, AJ, 128, 3034
- Kudritzki, R.P. 2002, ApJ, 577, 389
- Labbe, I., et al. 2003, AJ, 125, 1107
- Lamb, D.Q., & Reichart, D.E. 2000, ApJ, 536, 1
- Lawrence, A., et al. 2007, MNRAS, 379, 1599
- Lawrence, J.S. 2004, PASP, 116, 482
- Lawrence, J.S., Ashley, M.C.B., Travouillon, T. & Tokovinin, A. 2004, Nature, 431, 278
- Lawrence, J.S., et al. 2009a, PASA, submitted (Paper I)
- Lawrence, J.S., et al. 2009b, PASA, submitted (Paper III)
- Lewis, I., et al. 2002, MNRAS, 334, 673
- MacFadyen, A.I., & Woosley, S.E. 1999, ApJ, 524, 262
- Mackey, J., Bromm, V., & Hernquist, L. 2003, ApJ, 586, 1
- Maiolino, R., Vanzì, L., Mannucci, F., Cresci, G., Ghinassi, F., & Della Valle, M. 2002, A&A, 389, 84
- Manucci, F., Della Valle, M., & Panagia, N. 2007, MNRAS, 377, 1229
- Mobasher, B., et al. 2005, ApJ, 635, 832
- Mosser, B., & Aristidi, E. 2007, PASP, 119, 127
- Muñoz, J.A., & Loeb, A. 2008, MNRAS, 385, 2175
- Nousek, J. A., et al. 2006, ApJ, 642, 389
- Nozawa, T., Kozasa, T., Umeda, H., Maeda, K., & Nomoto, K. 2003, ApJ, 598, 785
- Perlmutter, S., et al. 1999, ApJ, 517, 565
- Pimblet, K.A., Smail, I., Edge, A.C., O'Hely, E., Couch, W.J., & Zabludoff, A.I. 2006, MNRAS, 366, 645
- Pozzo, M., et al. 2006, MNRAS, 368, 1169
- Prochaska, J.X., Chen, H.W., Dessauges-Zavadsky, M., & Bloom, J.S. 2007, ApJ, 666, 267
- Quadri, R., et al. 2007, AJ, 654, 138
- Refregier, A., et al. 2006, Proc. SPIE, 6265, 62651Y

- Rieke, G.H., & Lebofsky, M.J. 1985, *ApJ*, 288, 618
- Romer, A.K., Viana, P.T.P., Liddle, A.R., & Mann, R.G. 2001, *ApJ*, 547, 594
- Salvaterra, R., Campana, S., Chincarini, G., Covino, S., Tagliaferri, G. 2008, *MNRAS*, 385, 189
- Saunders, W., Gillingham, P., McGrath, A., Haynes, R., Brzeski, J., Storey, J., & Lawrence, J. 2008a, *Proc. SPIE*, 7012, 70124F1
- Saunders, W., Gillingham, P., McGrath, A., Haynes, R., Storey, J., Lawrence, J., Burton, M., & Mora, A. 2008b, *Proc. SPIE*, 7014, 70144N
- Scannapieco, E., Madau, P., Woosley, S., Heger, A., & Ferrara, A. 2005, *ApJ*, 633, 1031
- Scannapieco, E., Schneider, R., & Ferrara, A. 2003, *ApJ*, 589, 35
- Schmidt, B.P., et al. 1998, *ApJ*, 507, 46
- Smith, G.P., Treu, T., Ellis, R.S., Moran, S.M., & Dressler, A. 2005, *ApJ*, 620, 78
- Smith, N., & McCray, R. 2007, *ApJ*, 671, L17
- Smith, N., et al. 2007, *ApJ*, 666, 1116
- Smith, N., et al. 2008, *ApJ*, submitted, eprint (arXiv:0802.1743)
- Stott, J.P., Pimblet, K.A., Edge, A.C., Smith, G.P., & Wardlow, J.L. 2008, *MNRAS*, submitted
- Stott, J. P., Smail, I., Edge, A. C., Ebeling, H., Smith, G. P., Kneib, J.P., & Pimblet, K.A. 2007, *ApJ*, 661, 95
- Takeuchi, T.T., Buat, V., & Burgarella, D. 2005, *A&A* 440, L17
- Tomasi, C., et al. 2006, *J. Geophys. Res.*, 111, D20305
- Tonry, J.L., et al. 2003, *ApJ*, 594, 1
- Totani, T., & Panaitescu, A. 2002, *ApJ*, 576, 120
- Trinquet, H., Agabi, A., Vernin, J., Azouit, M., Aristidi, E., & Fossat, E. 2008, *PASP*, 120, 203
- Tyson, J.A., et al. 2006, *AIP Conf. Proc.*, 870, 44, eprint (astro-ph/0609516)
- van Dokkum, P.G., et al. 2006, *ApJL*, 638, L59
- van Dokkum, P.G., et al. 2007, Warm Spitzer Mission White Paper
- von Kienlin, A. et al. 2004, *Proc. SPIE*, 5488, 763
- Wake, D.A., Collins, C.A., Nichol, R.C., Jones, L.R., & Burke, D. J. 2005, *ApJ*, 627, 186
- Walden, V.P, Town, M.S., Halter, B., & Storey, J.W.V. 2005, *PASP*, 117, 300
- Weimann, S.M., & Lilly, S.J. 2005, *ApJ*, 624, 526
- Wise, J.H., & Abel, T. 2005, *ApJ*, 629, 615
- Williams, R.E., et al. 1996, *AJ*, 112, 1335
- Wood-Vasey, W.M. et al. 2007, *ApJ*, submitted, eprint (arXiv:0711.2068)
- Woosley, S.E., Blinnikov, S., & Heger, A. 2007, *Nature*, 450, 390
- Woosley, S.E. & Bloom, J.S. 2006, *ARA&A*, 44, 507
- Yahata, M., et al. 2000, *ApJ*, 583, 493
- Zhang, B., et al. 2006, *ApJ*, 642, 354
- Zou, Y.C., Wu, X.F., & Dai, Z.G. 2007, *A&A*, 461, 115